Effect of Scaling Transfer between Evapotranspiration Maps Derived from LandSat 7 and MODIS Images

Sung-ho Hong, Jan M.H. Hendrickx and Brian Borchers
New Mexico Tech, 801 Leroy place, Socorro, NM 87801, USA

ABSTRACT

Remotely sensed images of the Earth's surface provide information about the spatial distribution of evapotranspiration. Since the spatial resolution of evapotranspiration predictions depends on the sensor type; scaling transfer between images of different scales needs to be investigated. The objectives of this study are first to validate the consistency of SEBAL algorithms for satellite images of different scales and second to investigate the effect of up- and down-scaling procedures between evapotranspiration maps derived from LandSat 7 and MODIS images. The results of this study demonstrate: (1) good agreement of SEBAL evapotranspiration estimates between LandSat 7 and MODIS images; (2) up- and down-scaled evapotranspiration maps over the Middle Rio Grande Basin are very similar to evapotranspiration maps directly derived from LandSat 7 and MODIS images.

Keywords: Remote sensing, Scaling, Evapotranspiration, LandSat 7, MODIS

1. INTRODUCTION

Remote sensing using satellite-based sensors has the potential to provide detailed information on land surface properties and parameters over large areas[6,10,12,14]. Perhaps one of the most important land surface parameters that can be derived from optical remote sensing is evapotranspiration (ET). Since ET is an important component of the hydrologic cycle in arid environments, the determination of the spatial distribution of ET over a range of space and time scales is needed for sustainable management of water resources as well as for a better understanding of water exchange processes between the land surface and the atmosphere.

The scale or pixel size of remote sensing data is dependent upon the spatial resolution of its satellite imagery. In this study, two different satellite images will be used to examine the effect of scale transfer processes. The LandSat 7 Enhanced Thematic Mapper Plus (ETM+) launched in 1999 has 30m visible and 60m thermal band pixel size but poor temporal resolution (i.e. 16 days). More recently (2000), the Moderate Resolution Imaging Spectroradiometer (MODIS) is providing information of high temporal resolution (twice a day) but a coarse spatial resolution (250 to 500m in the visible and 1000x1000m in the thermal bands).

For an accurate prediction of water consumption at the field level homogeneous pixels with a single vegetation type are needed. Therefore, it seems that accurate estimates of water consumption can only be done using fine spatial resolution images like LandSat 7. However, LandSat 7 images are not suitable for global scale land surface characterization and monitoring. Although coarse resolution images like MODIS provide very useful opportunities to monitor the energy balance at meso scale, they cannot directly provide field specific data. Therefore, scaling transfer between LandSat 7 and MODIS is needed to take advantage of high temporal and various spatial resolutions of land surface parameters.

Many studies in the last decade have examined the effects of different pixel sizes[7,8,11,20,21]. Since most of these studies addressed up-scaling only, there is a need for more information on down-scaling procedures. The first objective of this paper is to assess the possible discrepancy of daily ET rates estimated using SEBAL through LandSat 7 and MODIS. The second objective is to implement various scaling transfer approaches for investigating the effect of the scaling transfer between ET maps derived from LandSat 7 and MODIS images.

Targets and Backgrounds XI: Characterization and Representation, edited by Wendell R. Watkins,
Dieter Clement, William R. Reynolds, Proceedings of SPIE Vol. 5811
(SPIE, Bellingham, WA, 2005) · 0277-786X/05/$15 · doi: 10.1117/12.603385

2. SCALING TRANSPER PROCESS

Although LandSat 7 and MODIS images differ in many ways, including wavelength of spectral bands, scanning system and sensitivity, the largest difference is in the spatial and temporal resolutions (Figure 1). One MODIS image can cover from the Gulf of California to the Gulf of Mexico while a LandSat image covers a much smaller area of about 160x160 km. The LandSat 7 images used in this study covered the Middle Rio Grande Basin (Path/Row: 34/36).

Scaling transfer means changing data or information from one scale to another. Upscaling consists of taking information at smaller scales to derive processes at larger scales, while downscaling consists of decomposing information at one scale into its constituents at smaller scales (Figure 2).

In the up-scaling process (LandSat 7 resolution to MODIS resolution on June 6, 2002), two different procedures were evaluated. The first consists of averaging 60 by 60m LandSat 7 pixels of the input parameter (radiance) to obtain 1000 by 1000 m pixels at the MODIS scale before SEBAL is applied. The second consists of first applying SEBAL and then averaging the output parameter (daily ET) from 60 m to 1000 m spatial resolution. In the averaging process, 60 by 60m pixels were broken into 10 by 10m pixels with the same pixel values and then were averaged into 1000 by 1000m pixels. The averaging process (aggregation) includes calculating arithmetic and geometric means.

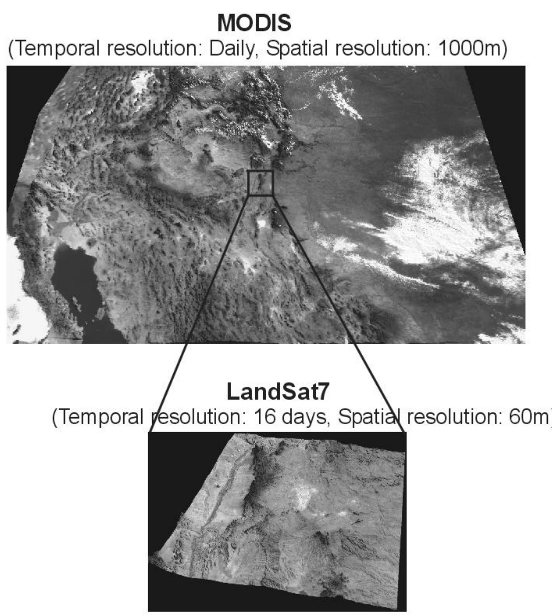

Figure 1. LandSat 7 and MODIS images have different spatial and temporal resolutions.

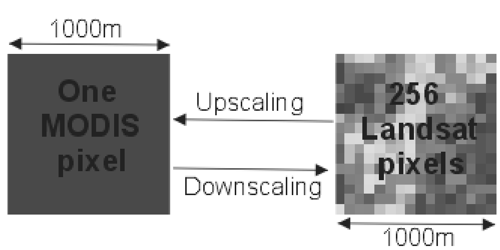

Figure 2. Scaling transfer between LandSat 7 and MODIS pixels.

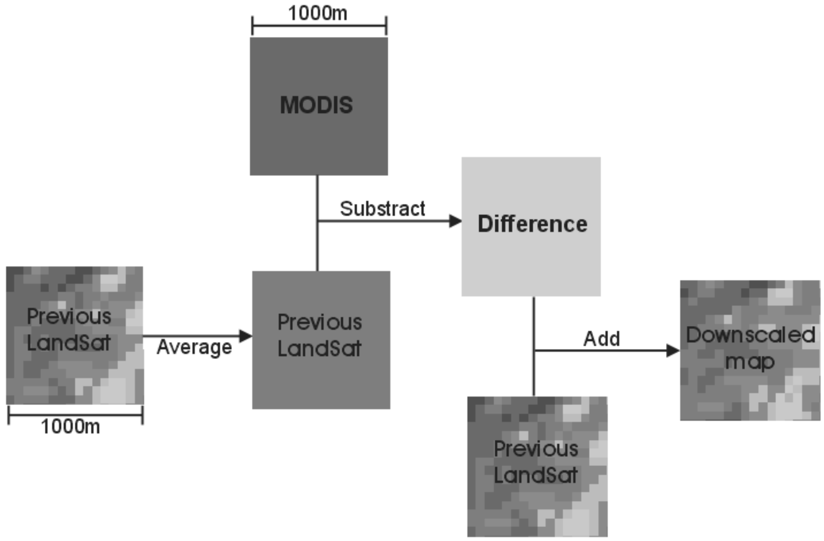

Figure 3. Flow diagram of the down-scaling procedure within one MODIS pixel with dimensions 1000x1000 m.

In the down-scaling process (disaggregation MODIS resolution to LandSat 7 resolution on June 16, 2002) (Figure 3), an earlier LandSat 7 image of May 31, 2002, was used to characterize the fine scale variability within the large MODIS pixels. Two down-scaling procedures were evaluated. The first consists of down-scaling the MODIS input parameter (radiance); the second of down-scaling the output parameter (daily ET) at MODIS resolution. Similar to up-scaling, 1000 by 1000m pixels were first down-scaled into 10 by 10m pixels and then averaged into 60 by 60m pixels.

3. SEBAL ALGORITHM

In this study, the Surface Energy Balance Algorithm for Land (SEBAL)[1]was used to derive evapotranspiration maps from LandSat 7 and MODIS images. The SEBAL method has been used in various studies to assess ET rates in Idaho, Spain, Italy, Turkey, Pakistan, India, Sri Lanka, Egypt, Niger, and China[1,2,16,19]. In this volume we have a companion paper by Hendrickx and Hong that describes an application of SEBAL in arid heterogeneous riparian areas of the southwestern United States

SEBAL is a physically based analytical method that evaluates the components of the energy balance and determines the ET rate as the residual

$$R_n - G - H = \lambda ET \qquad (1)$$

where R_n is the net incoming radiation flux density (Wm^{-2}), G is the ground heat flux density (Wm^{-2}), H is the sensible heat flux density (Wm^{-2}), λET is the latent heat flux density (Wm^{-2}), and parameter λ is the latent heat of vaporization of water (J kg^{-1}). The ET rates are determined as ET=$\lambda ET/\lambda$.

SEBAL is based on the computation of energy balance parameters from multi spectral satellite data. Table 1 shows the spectral bands of LandSat 7 and MODIS in the visible, near infrared and thermal infrared wavelength regions used in this study. The original spatial resolution of the visible and near infrared imagery of 30m in LandSat 7 and 250 and 500m in MODIS, was reduced to 60m and 1000m to be compatible with the resolution of the thermal imagery. Table 2 shows the spatial resolution of MODIS and LandSat 7.

Table 1. Spectral bands and their wavelengths (μm) used in SEBAL.

Sensors	Band								
	1	2	3	4	5#	6	7	31	32
LandSat 7	0.45 – 0.51	0.52 – 0.06	0.63 – 0.69	0.75 – 0.9	1.55 – 1.75	10.4 – 12.5	2.09 – 2.35	NA*	NA
MODIS	0.62 – 0.67	0.84 – 0.87	0.46 – 0.48	0.54 – 0.56	1.23 – 1.25	1.63 – 1.65	2.11 – 2.15	10.8 – 11.3	11.8 – 12.3

#MODIS band5 is not used in this study because of streaking noise, *Not available

Table 2. Spatial resolution of LandSat and MODIS sensors (m).

Sensors	Band								
	1	2	3	4	5	6	7	31	32
LandSat 7	30	30	30	30	30	60	30	NA	NA
MODIS	250	250	500	500	500	500	500	1000	1000

Since MODIS bands 1, 2, 3, 4, 6 and 7 are compatible with LandSat 7 bands 3, 4, 1, 2, 5 and 7, most of the SEBAL algorithms using MODIS are similar to the LandSat 7 algorithms. The only difference is the algorithm for surface temperature calculations. SEBAL uses one thermal band for surface temperature estimation through the LandSat 7 while two thermal bands are used for the MODIS application.

3.1 Brightness temperature

The temperature detected by a thermal sensor is called the brightness temperature. Radiance data from LandSat 7 and MODIS thermal infrared bands are first converted to brightness temperatures with an inversion of Planck's equation:

$$T_b = \frac{hc/k\lambda}{\ln\left(\frac{2hc^2\lambda^{-5}}{L_\lambda}+1\right)} = \frac{K_2}{\ln\left(\frac{K_1}{L_\lambda}+1\right)} \tag{2}$$

T_b is the brightness temperature in Kelvin [K], c is the speed of light (2.998 x 10^8) [ms^{-1}], h is the Planck's Constant (6.626 x 10^{-34}) [Js], k is the Boltzmann constant (1.3807 x 10^{-23}) [JK^{-1}], L_λ is the spectral radiance [Wm^{-2}μm^{-1}sr^{-1}], λ is the band effective center wavelength [μm] and K_1 and K_2 are calibration coefficients [Wm^{-2}sr^{-1}μm^{-1}] [LandSat 7 band6: K_1(666.09), K_2(1282.71); MODIS band31: K_1(730.01), K_2(1305.84) and band32: K_1(474.99), K_2(1198.29)].

3.2 Surface temperature

LandSat 7: If an object is a black body, its satellite-observed brightness temperature coincides with the surface temperature since the emissivity of a black body equals unity. However, objects on the earth surface are not perfect black bodies and they have emissivities less than unity. Therefore, the value of ε_0 should be known for the computation of the surface temperature. In this study, surface temperature (T_s) is estimated using T_b and ε_0 with the following empirical relationship[13].

$$T_s = \frac{T_b}{\varepsilon_0^{\ 0.25}} \tag{3}$$

where, $\varepsilon_0 = 1.009 + 0.47\ ln(NDVI)$[3].

MODIS: Split window algorithms take advantage of the differential absorption in two close infrared bands to account for the effects of absorption by atmospheric gases. Several split window algorithms are currently available to derive surface temperature from brightness temperature[4,9,15,17]. In this study the algorithm developed by Price[15] was applied since Vazquez et al. [18] claimed that it performed better than other algorithms:

$$T_s = T_{31} + 1.8(T_{31} - T_{32}) + 48(1-\varepsilon) - 75\Delta\varepsilon \tag{4}$$

where T_{31} is the brightness temperature obtained from band31 [K], T_{32} is the brightness temperature obtained from band 32 [K], $\varepsilon = (\varepsilon_{31} + \varepsilon_{32})/2$, $\Delta\varepsilon = \varepsilon_{31} - \varepsilon_{32}$, ε_{31} is the surface emissivity in band 31 and ε_{32} is the surface emissivity in band 32.

In 1997, Cihlar et al. [5]developed an algorithm to calculate the surface emissivity from NDVI.

$$\Delta\varepsilon = \varepsilon_{31} - \varepsilon_{32} = 0.01019 + 0.01344 \ln(NDVI) \tag{5}$$

where, $\varepsilon_{31} = 0.9897 + 0.029\ln(NDVI)$.

4. RESULTS AND DISCUSSION

4.1. Comparison of SEBAL ET rates derived from LandSat 7 and MODIS images

The SEBAL algorithms were applied to one LandSat 7 image and one MODIS image acquired on June 16, 2002, to estimate daily ET rates (Figure 4). Both the overall ET maps as well as the ET histograms match each other quite well which is an indication that the spatial resolution of an image doesn't affect much SEBAL derived ET rates. In the next section we will quantify some of the differences between the two ET maps.

Both of the ET images clearly show the high ET rates in the irrigated fields and riparian areas in the Rio Grande Valley and the low ET rates in the adjoining desert areas. The city of Albuquerque has a somewhat higher ET rate than its surroundings. The irrigated fields underneath the center pivot systems in the Estancia basin have a much higher ET than the bare fields surrounding them. The ET map derived from the LandSat 7 image shows a slightly higher ET mean and standard deviation than the one derived from the MODIS image. Many small areas (length scale on the order of 10 to 100 m) along the river and in the mountains have peak ET rates that are captured well in the LandSat derived ET map with spatial resolution of 30 m. However, these peak ET rates are averaged out on the MODIS derived ET map with spatial resolution of 1000 m.

4.2. Effect of up- and down-scaling

Figure 5 presents examples of scale transferred ET maps and their histograms. These scale transferred ET maps have good agreement with the original ET maps in Figure 4. Figure 6 presents the effect of up- and down-scaling as absolute ET difference maps between the original ET map derived directly from LandSat 7 and MODIS imagery and the one generated from scaling transfer. A few lines with apparently high ET differences are observed along the Rio Grande River riparian areas. These anomalies are due to errors with image registrations since the registration of two maps with spatial resolutions differing more than one order of magnitude is not trivial. It causes abrupt ET changes at the boundaries between riparian (high ET) and desert (low ET) areas. For example, to obtain completely accurate down-scaling results in Figure 3, the image registrations among the MODIS image of June 16, 2002, and the LandSat 7 images of May 31 and June 16, 2002, should be perfect.

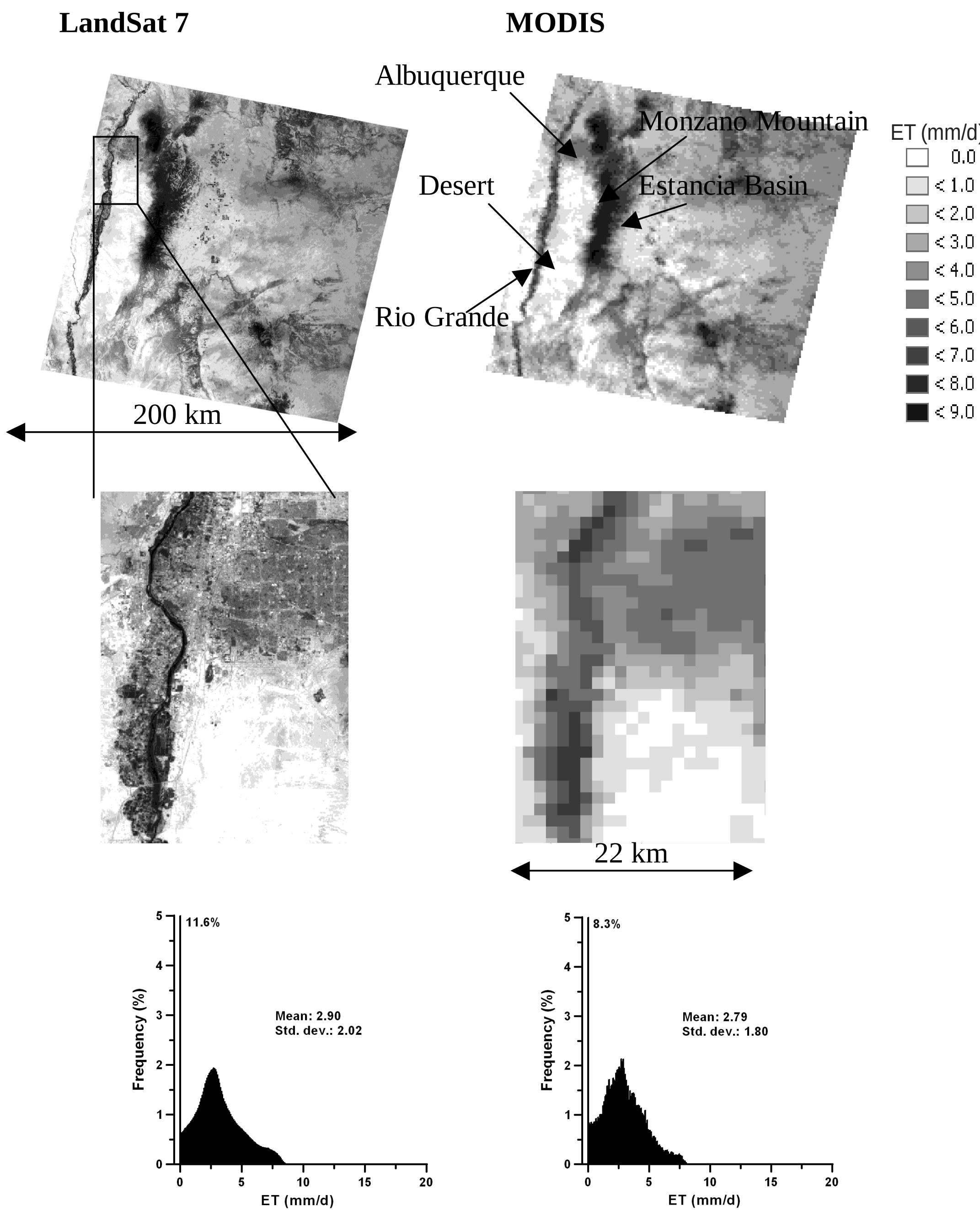

Figure 4. Evapotranspiration maps derived from LandSat 7 and MODIS on June 16, 2002. The enlarged areas show the details provided by, respectively, the LandSat and MODIS derived ET maps. The histograms are based on the entire maps.

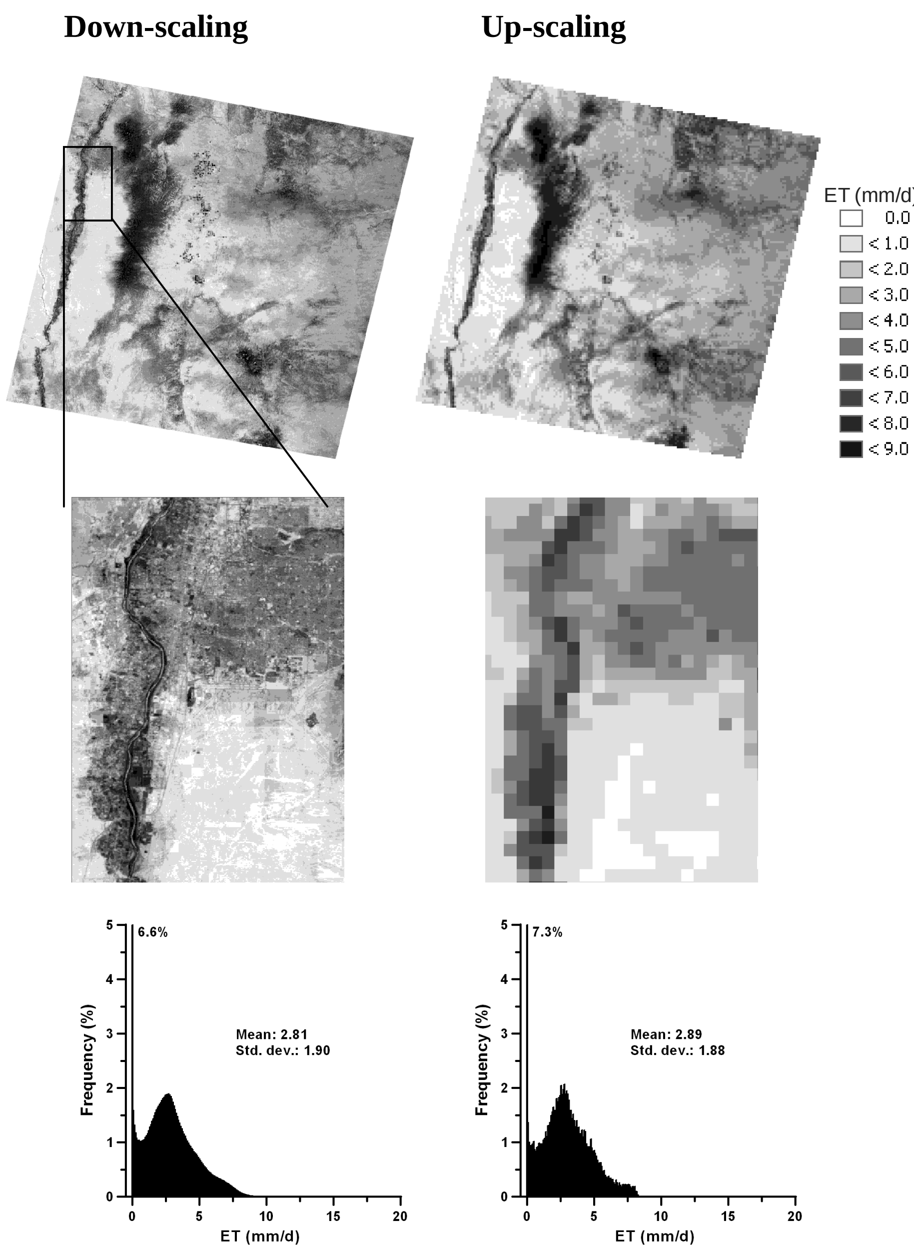

Figure 5. Evapotranspiration maps derived from output down-scaling (left) and output up-scaling (right). The enlarged areas show the details provided by, respectively, down- and up-scaling. Comparing these enlarged areas with those in Figure 4 provides a qualitative measure for the quality of the down- and up-scaling procedures. The histograms are based on the entire maps.

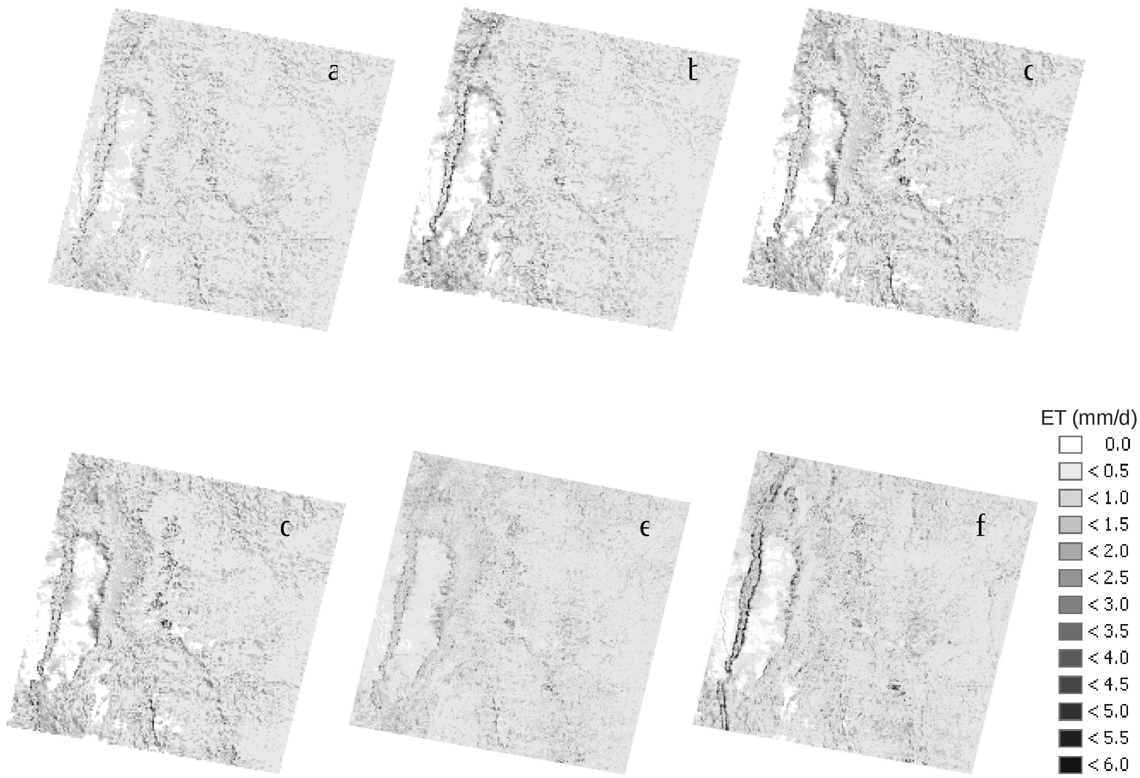

Figure 6. Maps of ET differences between the original ET map derived either from the LandSat 7 or MODIS images on June 16, 2002, and the up- or down-scaled ET maps. (**a**) Output up-scaling using arithmetic average; (**b**) Output up-scaling using geometric average; (**c**) Input up-scaling using arithmetic average; (**d**) Input up-scaling using geometric average; (**e**) Output down-scaling; (**f**) Input down-scaling.

Figure 7 presents the histograms of the ET differences shown on the maps in Figure 6. In the up-scaling results, means of the ET difference range from 0.45 to 0.60 mm/day and standard deviations range from 0.42 to 0.60 mm/day. Means and standard deviations of the down-scaling results are slightly higher and range from 0.54 to 0.60 mm/day and 0.51 to 0.65 mm/day, respectively. In the up-scaling procedures only a slight difference exists between arithmetic and geometric means. In both up- and down-scaling procedures, output scaling transfer performs better. All histograms of ET differences show similar shapes and the dominance of zero values.

Figure 8 presents maps of the relative errors $[(ET_{original} - ET_{scaled})/ET_{original} * 100]$ as well as three dimensional graphs of the relationship between relative error and daily ET rate. The areas having zero ET in the original map are assigned to be 100% relative errors. Large relative errors (> ~75%) occur in areas having low ET (< ~2 mm/d) while areas having ET greater than 2 mm/d exhibit relative errors less than 25%. For the downscaling procedure there are some points having 100% relative error with high daily ET. However, these points are the result from the anomalies resulting from registration errors as discussed above.

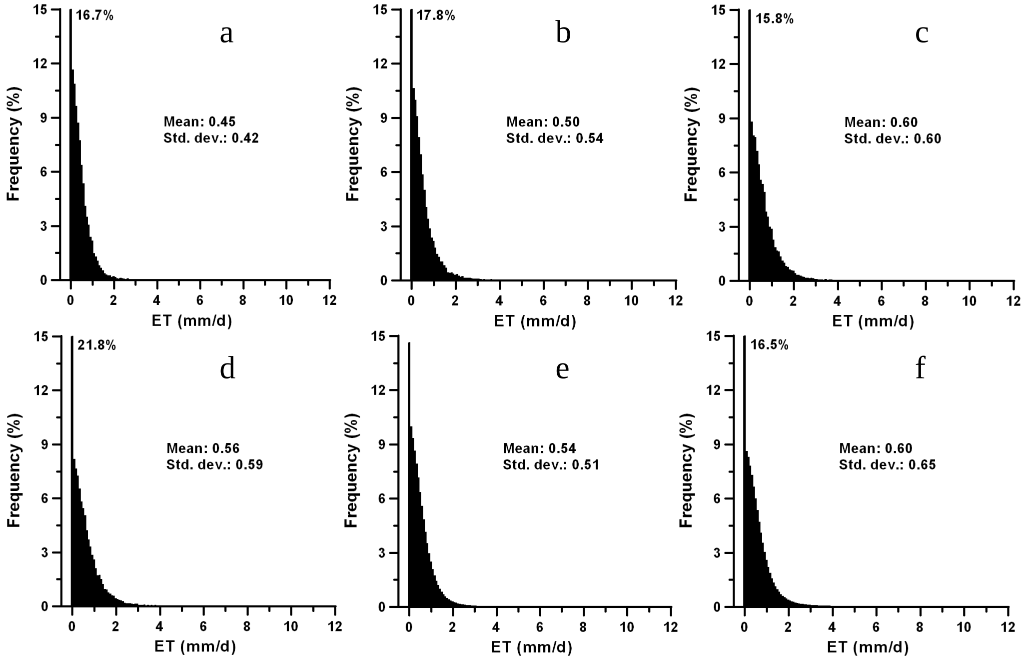

Figure 7. Histograms of ET differences between the original ET map derived either from the LandSat 7 or MODIS images on June 16, 2002, and the up- or down-scaled ET maps. (**a**) Output up-scaling using arithmetic average; (**b**) Output up-scaling using geometric average; (**c**) Input up-scaling using arithmetic average; (**d**) Input up-scaling using geometric average; (**e**) Output down-scaling; (**f**) Input down-scaling.

5. CONCLUSIONS

In this study, first daily evapotranspiration rates were calculated using SEBAL algorithms with LandSat 7 and MODIS imagery and then up- and down-scaling procedures were used to investigate the effect of scaling transfer on evapotranspiration maps. Preliminary results are:

1. Evapotranspiration maps derived from LandSat 7 (60 m scale) and MODIS (1000 m scale) images are very similar.

2. Up-scaling produces somewhat better results than down-scaling.

3. Output scaling transfer performs slightly better than input scaling transfer.

4. Large relative errors occur in desert areas with low to zero ET rates; areas having high ET rates show small relative errors.

5. Overall, the up- and down-scaled ET maps over the Middle Rio Grande Basin are in good agreement with ET maps directly derived from LandSat 7 and MODIS images.

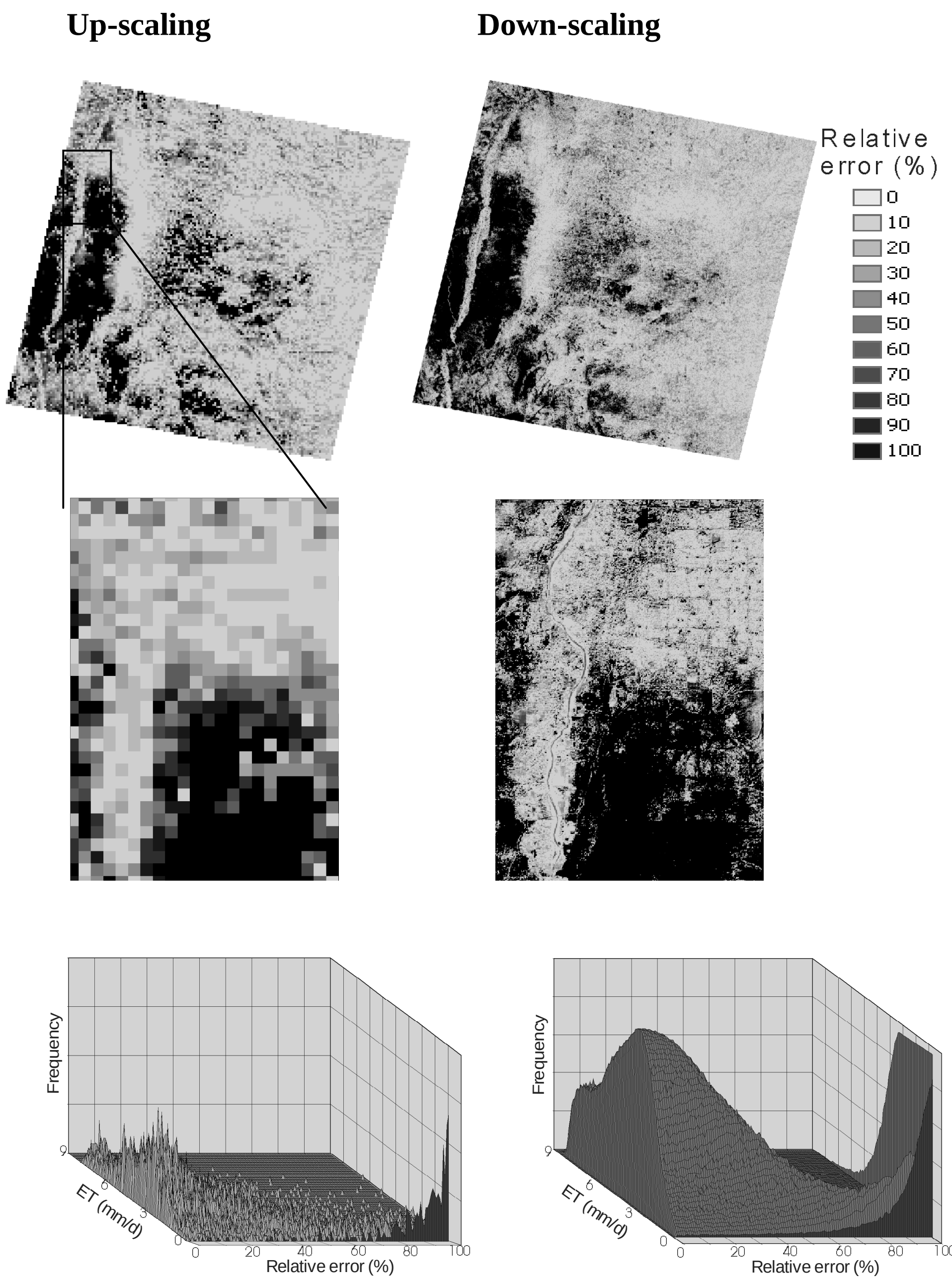

Figure 8. The left-hand side of the figure refers to output up-scaling using arithmetic average and the right-hand side to output down-scaling on June 16, 2002. The two top maps show the relative error maps for the entire image while the two lower maps show details for the enlarged area. The bottom line presents the relationships between relative error, ET rate, and frequency of occurrence.

ACKNOWLEDGEMENT

Because of the steep learning curve for SEBAL we have worked on this study more than five years. We are grateful to our past sponsors for their patience and current sponsors for the opportunity to further develop SEBAL and its applications for hydrology and mobility studies. The following sponsors have contributed to this study: U.S. Department of Agriculture, CSREES grant No.: 2003-35102-13654; Institute of Natural Resources Analysis and Management (INRAM) funded by NSF EPSCoR grant EPS-0132632; New Mexico Universities Collaborative Research (NUCOR) program for joint research with the Los Alamos National Laboratory; and the NSF Science and Technology Center program Sustainability of Semi-arid Hydrology and Riparian Areas (SAHRA; EAR-9876800).

REFERENCES

1. Bastiaanssen, W.G.M., M. Menenti, R.A. Feddes, and A.A. M. Holtslag. 1998a. *A remote sensing surface energy balance algorithm for land (SEBAL). Part 1: Formulation*. Journal of Hydrology 212-213:198-212.
2. Bastiaanssen, W.G.M., H. Pelgrum, J. Wang, Y. Ma, J.F. Moreno, G.J. Roerink, R.A. Roebeling, and T. van der Wal. 1998b. *A remote sensing surface energy balance algorithm for land (SEBAL). Part 2: Validation.* Journal of Hydrology 212-213:213-229.
3. Bastiaanssen, W.G.M. 2000. *SEBAL-based sensible and latent heat fluxes in the Irrigated Gediz Basin, Turkey.* Journal of Hydrology 229:87-100.
4. Becker, F., and Z.L.Li. 1990. *Towards a local split window method over land surface.* International Journal of Remote Sensing. 3:369-393
5. Cihlar, J., H. Ly, Z. Li, J. Chen, H. Pokrant, and F. Hung. 1997. *Multi-temporal, Multi-channel AVHRR data sets for land biosphere studies – Artifacts and corrections*. Remote Sensing of Environment. 60: 35-57.
6. Diak, G.R. and T.R. Stewart.1989. *Assessment of surface thrbulent fluxes using geostationary satellite surface skin temperature and a mixed layer planetary boundary layer scheme.* Journal of Geophyical Research. 94: 6357-6373.
7. Hay, G.J., K.O. Niemann and D.G. Goodenough. 1997. *Spatial thresholds, image-objects, and upscaling: A multiscale evaluation.* Remote Sensing of Environment. 62:1-19.
8. Heuvelink, G.B.M. and E.J. Pebesma. 1999. *Spatial aggregation and soil process modeling.* Geoderma. 89:47-65.
9. Keer, Y.H., J.P. Lagouarde, and J. Imbernon. 1992. *Accurate land surface temperature retrieval from AVHRR data with use of an improved split window*. Remote Sensing of Environment. 41:197-209
10. Kustas, W.P. and K.S. Humes 1996. *Sensible heat flux from remotely-sensed data at different resolutions.* In: Scaling up in Hydrology using Remote Sensing. J.B. Stewart, E.T. Engman, R.A. Feddes and Y. Kerr (Ed), John Wiley & Sons: 127-145.
11. Marceau, D.J., P.J. Howarth and D.J. Gratton. 1994. *Remote sensing and the measurement of geographical entities in a forested environment 1) the scale and spatial aggregation problem.* Remote Sensing of Environment. 49:93-104.
12. McCabe, M.F., S.W. Franks and J.D. Kalma. 2001. *Improved conditioning of SVAT models with observations of infrared surface temperatures.* In: Soil Vegetation Atmosphere Transfer Schemes and Large Scale Hydrological Models. A.J. Dolman, A.J. Hall, M.L. Kavvas, T. Oki and J.W. Pomeroy (Ed). Wallingford, UK., Int. Assoc. of Hydrol. Sci. (IAHS). Publ. 270:217-224.
13. Morse, A., M. Tasumi, R.G. Allen and W.J. Kramer. 2000. *Application of the SEBAL methodology for estimating consumptive use of water and streamflow depletion in the Bear river basin of Idaho through remote sensing.* Report Idaho Department of Water Resources, University of Idaho.
14. Nunez. M. and J.D. Kalma 1996. *Satellite mapping of the surface radiation budget.* In: Advances in Bioclimatology. G. Stanhill (Ed). Berlin, Springer-Verlag: 63-124.
15. Price, J.C. 1984. *Land surface temperature measurements from the split window channel of the NOAA 7 Advanced Very High Resolution Radiometer*. Journal of Geophysical Research. 89: 7231-7237.
16. Timmermans, W.J., A.M.J. Meijerink and M.W. Lubczynski. 2001. *Satellite derived actual evapotranspiration and groundwater modeling, Botswana*. Remote Sensing in Hydrology 2000 (Proceedings of a symposium held at Santa Fe, New Mexico, USA, April 2000). IAHS Publ. no. 267, 2001, ISSN 0144-7815: 2520258.

17. Ulivieri, C., M.M. Castromouvo, R. Francioni, and A. Cardillo. 1992. A split window algorithm for estimating land surface temperature from satellite. Advances in Space Research. 14:59-65
18. Vazquez, D.P., F.J. Olmo Reyes and L.A. Arboledas. 1997. *A comparative study of algorithms for estimating land surface temperature from AVHRR data*. Remote Sensing of Environment. 62: 215-222.
19. Wang, J., W.G.M Bastiaanssen, Y. Ma, and H. Pelgrum. 1998. *Aggregation of land surface parameters in the oasis-desert systems of Northwest China*. Hydrological Processes 12:2133-2147.
20. Wickham, J.D. and K.H. Riiters. 1995. *Sensitivity of landscape metrics to pixel size*. International Journal of Remote Sensing. 16: 3585-3594.
21. Woodcock, C.E., A.H. Strahler and D.L.B. Jupp. 1988. *The use of variograms in remote sensing: II. Real digital images*. Remote Sensing of Environment. 25: 349-379.